The Structure of Lithiated Aminonitriles in Solution: Interpretation of their Experimental IR Spectra by Means of *ab initio* Calculations *

Gerhard Raabe, Elke Zobel, Jörg Fleischhauer, Peter Gerdes, Dietrich Mannes, Edwin Müller, and Dieter Enders

Institut für Organische Chemie, Rheinisch-Westfälische Technische Hochschule Aachen, Aachen, FRG

Z. Naturforsch. **46a**, 275–288 (1991); received January 27, 1990

Quantum chemical calculations of relative energies and vibrational frequencies have been performed in order to elucidate the structure of metalated aminonitriles $(^1R^2RN)^3RC_2NLi$ formed upon lithiation of $(^1R^2RN)^3RCH-CN$ in tetrahydrofuran at −78 °C. For the sake of feasibility the calculations have been performed on model compounds where the heavy substituents ^1R, ^2R and ^3R and in some cases even the complete amino group $(^1R^2RN)$ and ^3R have been replaced by hydrogen atoms.

In the gasphase a lithium-bridged (nonclassical) monomer, whose lithium atom is within bonding distance to the atoms of the cyano group and the adjacent carbon atom, was found to be about 9 kcal/mol lower in energy than the most stable isomer of the corresponding nitrogen metalated ketenimine with amost linear CNLi moiety. However, the relative stability of the two structures will most likely be reversed under the influence of a solvent (modeled by H_2O).

Dimerization of H_2C_2NLi, yielding a product of D_{2h} symmetry with a four-membered $(LiN)_2$ ring, turned out to be exothermic by about 41 kcal/mol in the gasphase and 15 kcal/mol when the model solvent is present.

While in the case of the lithiated amino ketenimine with almost linear CNLi segment the structure obtained with the semiempirical MNDO method widely parallels the *ab initio* results, the semiempirical method seems to perform less reliably for the nonclassical monomer.

Formation of the trapping products obtained with methyl iodide and acetyl chloride is explained in terms of orbital- and charge control, respectively. According to this analysis, the results of trapping experiments are compatible with presence of a dimer, of a monomer with almost linear CNLi moiety, or of a monomer with lithium in a bridging position. However, comparison of observed and computed vibrational frequencies and of the calculated energies of classical and nonclassical structures led to the conclusion that the observed IR spectra are not due to nonclassical molecules with lithium in a bridging position. Taking into account the results of recent cryoscopic measurements we assign the characteristic absorptions in the experimental IR spectra to ketenimine-like monomers and their dimers.

1. Introduction

α-Aminonitriles of the general structure $(^1R^2RN)^3RCH-CN$ (cf. Scheme 1) undergo reaction with lithium diisopropylamide in ether at −78 °C, resulting in lithiated aminonitriles $(^1R^2RN)^3RC_2NLi$, which are synthetically useful acyl anion equivalents [1].

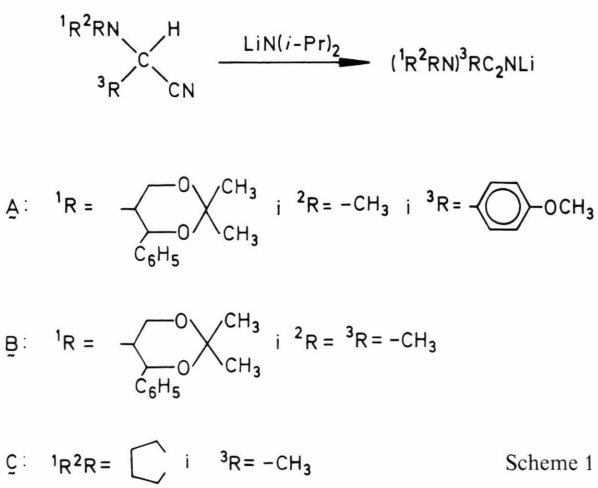

Scheme 1

* Presented in part by one of the authors (G.R.) at the 26th Symposium on Theoretical Chemistry, September 4–7, 1990, Alpbach, Austria.

Reprint requests to Prof. Dr. Jörg Fleischhauer, Lehr- und Forschungsgebiet Theoretische Chemie, Rheinisch-Westfälische Technische Hochschule Aachen, Professor-Pirlet-Straße 1, D-5100 Aachen.

0932-0784 / 91 / 0300-0275 $ 01.30/0. – Please order a reprint rather than making your own copy.

In tetrahydrofuran (THF) the metalated aminonitriles cause intense IR absorptions between 2000 and 2100 cm^{-1}, which fall into the range usually specified for ketenimines [2]. Nevertheless, the structure of the absorbing species is by no means obvious. Stuctural possibilities are, e.g., a lithiated ketenimine like **1**, a lithium-bridged (nonclassical) structure like **2**, or a dimer of **1** like **3** (cf. Scheme 2).

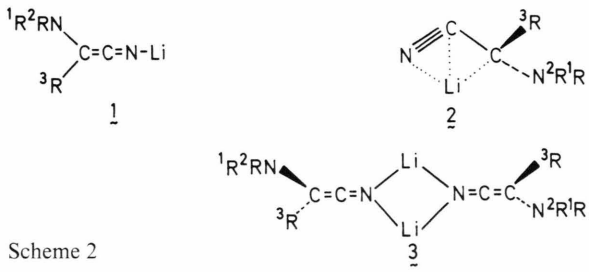

Scheme 2

According to a recent X-ray structure determination [2] the lithiated aminonitrile **A** forms a dimer **3** in the solid state, but this, of course, does not necessarily mean that association of the two units persists in solution.

Although the tendency of lithium compounds to form oligomers not only in solution but also in the gasphase is notorious [3], the degree of association in solution is a sensitive function of the substituents ^1R, ^2R, and ^3R, of the nature of the solvent, and of the temperature [4]. Thus, e.g., lithiated acetonitrile (**D**, $^1R^2RN$- and ^3R replaced by hydrogen) dissolved in THF, is a dimer between the melting point of the solvent and room temperature [5]. However, in the case of $C_6H_5CHCNLi$ in THF at $-108\,°C$ the monomer/dimer ratio is clearly in favour of the monomer [5–7], while the same compound seems to be a dimer in dimethyl sulfoxide [8]. The X-ray structure determination of lithiated phenyl acetonitrile complexed by tetramethylethylenediamine revealed that this molecule crystallizes as a dimer together with one molecule benzene in the asymmetric unit. In the solid state each lithium atom is coordinated by four nitrogen atoms, two being the termini of the α-cyanobenzyl units, while the other two are provided by the complexing tetramethylethylenediamine molecule [6].

We prepared lithiated aminonitriles **A**–**C** (cf. Scheme 1) and in the case of the compound with the largest substituents (**A**) a cryoscopic investigation revealed that this compound is widely monomeric under the conditions of the measurement. As jet no cryoscopic data are available for **B** and **C** [2].

Attempts to trap the metalated aminonitrile with H_3CCOCl resulted in N-acetyl ketenimine $(^1R^2RN)(^3R)C{=}C{=}N{-}COCH_3$, while reaction with H_3CI yielded the carbon-methylated compound $(^1R^2RN)^3RCH_3C{-}CN$ (cf. Scheme 3) [9].

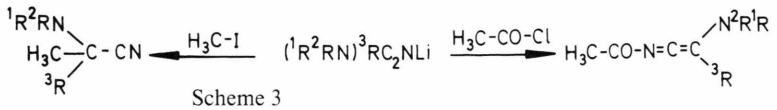

Scheme 3

The results are compatible with trapping of a ketenimine-like structure similar to **1**, the hard acid H_3CCOCl attacking the hard basic center of the molecule (i.e. nitrogen ^2N in, e.g., **1a**, cf. Fig. 1), while the softer electrophile H_3CI preferably reacts with the softer basic center ^4C. However, the same trapping products cannot only be derived from structures like lithiated ketenimine **1**, but also from the bridged molecule **2**. In addition the dimer **3** has to be taken into account as a possible source of the trapping product, since it might either be attacked directly by the trapping agents or be funneled off via equilibrium amounts of the monomer.

NMR spectroscopy of, e.g., isotopically labeled organolithium compounds (^6Li, ^{15}N, ^{13}C) is a powerful tool in determining their structure in solution [3, 10]. Our point in question was whether such problems can also be solved by means of standard IR spectroscopy. Thus, we recorded the infrared spectra of compounds **A**–**D** and interpreted them by comparison with calculated vibrational frequencies. Since the position of the stretching of the CCN segment in the IR spectrum of the complexed dimer of lithiated phenyl acetonitrile [6] which occurs in nujole at 2065 cm^{-1} is not too different from the absorptions obtained from the lithiated aminonitriles in THF [1], one might argue that these species are also dimers in solution. Since this argument convinces only if one can exclude that **1** and **2** show characteristic absorptions close to those of the dimer, we calculated the vibrational frequencies of model compounds. In these model compounds the main features of the possible structures were retained but the heavy substituents ^1R, ^2R, and ^3R and in some cases the entire amino group and ^3R were replaced by hydrogen atoms. Splitting of the characteristic absorption observed for some compounds attracted our special interest. A similar split-

ting had previously been observed for lithiated acetonitrile in THF [11, 12] and was assigned to simultaneous presence of free carbanions and solvent-separated ion pairs [11, 12].

In addition we performed quantum chemical calculations regarding the relative energies of nonclassical and ketenimine-like structures including a rough estimate of the solvent effect.

Another subject of interest was the influence of solvation on the dimerization energy of **1d** and **2b**, yielding **3a** (cf. Figure 1).

In addition we performed some explorative calculations with the semiempirical MNDO method on **1a**, **2a**, and the dimer of **C**.

2. Computational Method

Most calculations have been performed on the CDC Cyber 175 and IBM 3090 computer systems of the Rechenzentrum der Rheinisch-Westfälischen Technischen Hochschule Aachen employing the HONDO 5 [13] and GAMESS [14] *ab initio* program packages. Additional calculations with the Gaussian 86 [15] program have been performed on a TRACE computer. In all but one calculations, the correlation energy has been included in single point post SCF computations employing Møller-Plesset perturbation theory [16] to the second order (MP2) excluding inner shells. In the case of **2b**, geometry optimization has also been performed including MP2 corrections.

Starting from reasonable initial geometries, most of the molecules under consideration were preoptimized with the STO-3G and STO-6G basis sets [17]. The geometries obtained at this degree of accuracy served as starting points for further optimization with the split valence 3-21G [18] and 6-31G [19–21] sets of basis functions and the polarized 6-31G* basis set [22], which includes one set of d functions for all heavy atoms. In addition we used the 6-311G basis set, which has a triple split in the valence s and p shells, combined with an inner shell representation by a single function with six gaussians [23] (valence triple zeta).

Starting from a set of coordinates defined by means of X-ray data obtained from dimeric **A** [2] (cf. Table 11 of the appendix), the structure of **3a** has been optimized at the HF/6-31G* level under constraint of D_{2h} symmetry.

Except those of the solvated structures, all stationary points located with the STO-3G, the 6-31G, and the 6-31G* basis sets were characterized as either minima or saddle points by checking the eigenvalues of the cartesian force constant matrices.

For most of the MNDO [24] calculations we used a modified version of the standard MNDO program [25]. The vibrational spectra of the dimers of **C** have been calculated employing the MOPAC program package [26].

3. Results and Discussion

The stationary points obtained with the basis sets mentioned above are schematically drawn in Figure 1. Three perspective views of cyclic structure **2a** are displayed in Figure 2. The total and relative energies are listed in Tables 1 and 2, while most structural parameters are compiled in Tables 9–13 of the appendix.

With the STO-3G basis set, **1a** and **2a** turned out to be minima while **1b** and **1c** are saddle points, each yielding one imaginary number in the calculations of their vibrational frequencies. However, at the 6-31G level besides **1a** and **2a**, also **1c** is a local minimum, while starting from various sets of coordinates no stationary point corresponding to **1b** could be located with this basis set. All attempts to optimize the structure at this level resulted in **1a**.

3.1. Energetics

Our MP2/6-31G*//6-31G* results reveal that in the gasphase **2a** is 8.8 kcal/mol more stable than **1a**. Inclusion of zero point vibrational energy calculated at the HF/6-31G*//6-31G* level slightly reduces this difference to 8.6 kcal/mol. This value is somewhat smaller than 9.7 kcal/mol obtained for the energy difference between **1d** and **2b** [5]. Thus, the effect of the amino group is to reduce the energy difference between the ketenimine-like and the nonclassical structures.

To estimate the influence of the solvent on the relative stabilities of ketenimine-like and nonclassical systems we modeled the solvent by water molecules and calculated the changes of energy associated with the following reactions:

$$\underline{1d} + H_2O \longrightarrow \underline{1d}{*}H_2O$$

$$\underline{1d}{*}H_2O + H_2O \longrightarrow \underline{1d}{*}2H_2O$$

$$\underline{1d}{*}2H_2O + H_2O \longrightarrow \underline{1d}{*}3H_2O$$

Scheme 4

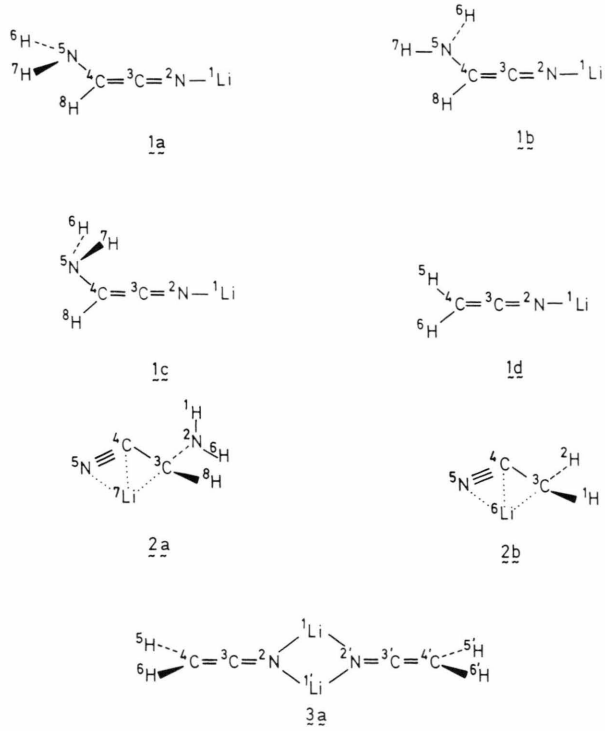

Fig. 1. Stationary points found for the model compounds under consideration [a].

The corresponding values are given in Table 3. Our MP2/6-31 G*//6-31 G* solvation energies for **1 d** are more negative than those obtained with the MNDO method [5], which, on the other hand, are more similar to our HF/6-31 G*//6-31 G* results. While the use of water molecules as a solvent model is applicable in the case of **1 d**, it fails for **2 b**. All attempts to optimize the geometry of **2 b** with a single water molecule attached to its lithium atom resulted in a structure which contains an internal O–H–N bridge (cf. Fig. 7 of the appendix). Something like this is not to be expected for the solvents actually used in the experiments, and thus the energies of the adducts **2 b** · nH_2O cannot be used for our purpose [c]. To overcome this problem and to get at least a rough estimate we assumed that the number of vacant positions in the coordination polyhedron of lithium is one less in **2 b** than in **1 d**. Consequently, if there are, e.g., two molecules of the solvent attached to the lithium atom in the ketenimine-like monomer, there will be one in the corresponding nonclassical structure. Roughly estimating that the actual energy changes associated with the processes

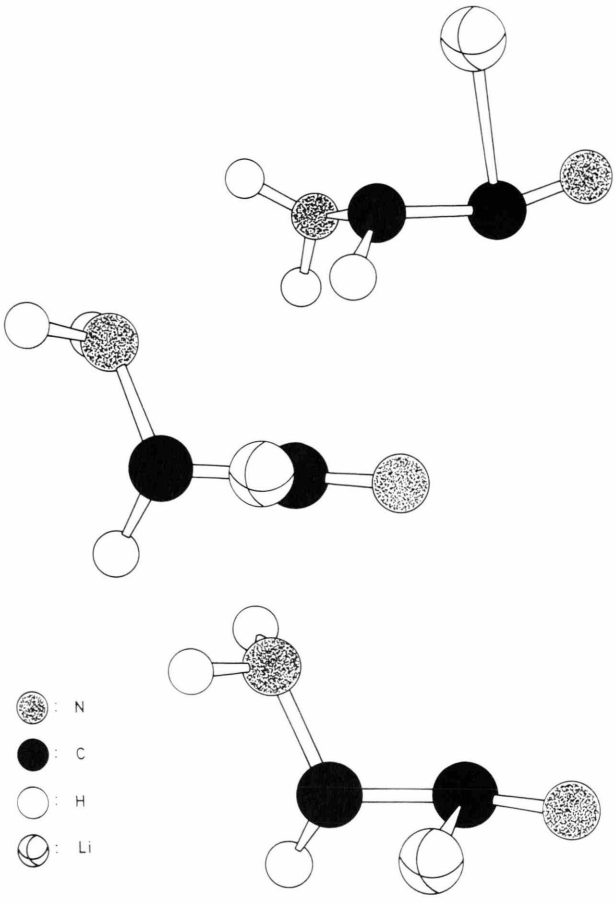

Fig. 2. Three perspective views of **2 a**.

[a] The representation of the four-membered rings of compounds **3 a** and **3** in Fig. 1 and Scheme 2 means a superposition of the two equivalent structures:

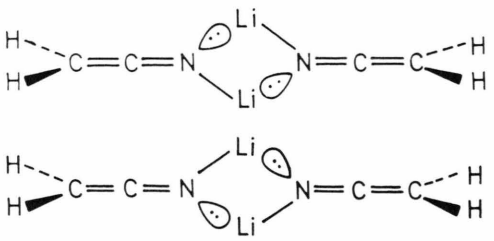

The dotted lines in **2**, **2 a** and **2 b** indicate that the lithium atom is also in what might be considered as bonding distances to ^5N and ^3C.

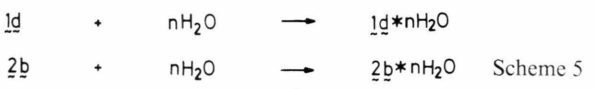

Scheme 5

[c] Attempts to find an additional minimum on the H_2C_2NLi hypersurface by optimization of the **2 b** part of this adduct met with failure. Reoptimization starting from this point resulted in **2 b**.

Table 1. Total energies of compounds under consideration (in a.u.). The values in parentheses are zero point energies calculated with the 6-31 G* basis set (in kcal/mol).

	1a	**1b**	**1c**	**1d**	**2a**
HF/STO-3G//STO-3G	−191.29208	−191.28875	−191.28983		−191.31284
HF/STO-6G//STO-6G	−193.17855	−193.17523	−193.17641		−193.19858
HF/6-31G//6-31G	−193.71742		−193.71610		−193.70662
HF/6-31G*//6-31G	−193.78599				−193.79261
HF/6-31G*//6-31G*	−193.78895		−193.78693	−138.77495 [b]	−193.79627
	(35.2)		(35.1)	(22.4)	(35.4)
HF/6-311G//6-311G	−193.76401		−193.76243		−193.75330
MP2/6-31G*//6-31G*	−194.36531		−194.36430	−139.18912 [b]	−194.37928
	2b	**1d** · H_2O	**1d** · $2H_2O$	**1d** · $3H_2O$	**2b** · H_2O
HF/3-21G//3-21G		−213.65530	−289.28675	−364.90448	−213.65847
HF/6-31G*//6-31G*	−138.78426 [b]	−214.82340	−290.86257	−366.89291	−214.83688
	(23.1)				
MP2/6-31G*//6-31G*	−139.20455 [b]	−215.42623	−291.65671	−367.87836	
	3a	**3a** · H_2O	**3a** · $2H_2O$		
HF/6-31G*//6-31G*	−277.64345	−353.68660	−429.72776		
	(47.3)				
MP2/6-31G*//6-31G*	−278.47459				

[b] From Ref. [5].

Table 2. Energies of $H_3C_2N_2Li$ isomers relative to the most stable species. The values in parentheses include zero point vibrational energies calculated at the 6-31 G*//6-31 G* level (in kcal/mol).

	1a	**1b**	**1c**	**2a**
HF/STO-3G//STO-3G	13.0	15.1	14.4	0.0
HF/STO-6G//STO-6G	12.6	14.6	13.9	0.0
HF/6-31G//6-31G	0.0		0.8	6.8
HF/6-31G*//6-31G	4.2			0.0
HF/6-31G*//6-31G*	4.6 (4.4)		5.9 (5.6)	0.0
HF/6-311G//6-311G	0.0		1.0	6.7
MP2/6-31G*//6-31G*	8.8 (8.6)		9.4 (9.1)	0.0

Table 3. Energy changes associated with the reactions **1d** · $(n-1)\,H_2O + H_2O = $ **1d** · $n\,H_2O$. All values in kcal/mol. (Total energies of water; HF/3-21G//3-21G: −75.58596 a.u.; HF/6-31G*//6-31G*: −76.01075 a.u.; MP2/6-31G*//6-31G*: −76.19596 a.u.)

	$n=1$	$n=2$	$n=3$
HF/3-21G//3-21G	−37.7	−28.5	−19.9
HF/6-31G*//6-31G*	−23.7	−17.8	−12.3
MP2/6-31G*//6-31G*	−25.8	−21.7	−16.1

will be the same [5], we conclude from the numbers in Table 3 that the bridged compound will be less stabilized in solution than **1d**.

As to be expected, **1c** (which in contrast to the STO-3G results is also a minimum on the 6-31G hypersurface of $H_3C_2N_2Li$) is almost isoenergetic with **1a**.

Our semiempirical calculations are based on the set of MNDO parameters for lithium taken from [27]. Using this parametrization [d], we located the two stationary points **1a′** and **2a′** (cf. Tables 12 and 13).

Obtaining the heats of formation ΔH_f(**1a′**) = 32.8 kcal/mol and ΔH_f(**2a′**) = 17.8 kcal/mol, carbon-lithiated **2a′** turned out to be 15.0 kcal/mol lower in energy than nitrogen-lithiated ketenimine **1a′**. This is more than three times the value obtained for the difference between **1a** and **2a** at the HF/6-31G*//6-31G* level of *ab initio* theory (cf. Table 2). On the other hand, this value is not too far from those obtained for the energy differences between **1a** and **2a** and between **1d** and **2b** on the MP2/6-31G*//6-31G* level.

3.2. Geometries

Discussion of the geometries will be focussed on the main structural parameters. More detailed information, as, e.g., basis set dependencies, may be extracted from Tables 9–13 of the appendix.

The $^2N^3C^4C$ moiety in **1a** is linear, while with an angle of 172.7° at ^2N, (6-31 G*) the $^1Li^2N^3C$ segment

[d] For the one-center repulsion integral (pp′, pp′), not specified explicitly in the parameter list [27], we calculated a value of 0.24 eV from (pp, pp) = 5.00 eV and (pp, p′p′) = 4.52 eV, making use of the relationships (pp, pp) = $F^0 + (4/25)\,F^2$, (pp, p′p′) = $F^0 - (2/25)\,F^2$, and (pp′, pp′) = $(3/25)\,F^2$. For the heat of formation for the free lithium atom we used ΔH_f = 38.41 kcal/mol.

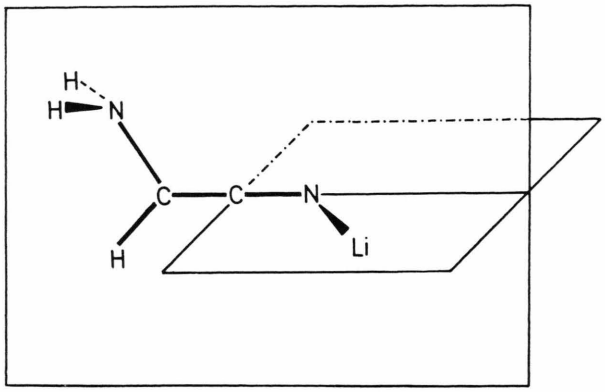

Fig. 3. Expected structure of lithiated ketenimine in case of sp^2 hybridized ^{2}N.

is slightly bent but still close to linearity. The almost linear arrangement of the atoms ^{1}Li, ^{2}N, and ^{3}C indicates sp hybridization of ^{2}N, resulting in donation of the nitrogen lone pair into an empty 2p orbital of the metal atom as frequently described in literature [28, 29]. sp^2 hybridization of ^{2}N would lead to a structure with a more pronounced CNLi bond angle and the Li atom lying in a plane orthogonal to the one defined by atoms ^{5}N, ^{3}C, and ^{8}H as shown in Figure 3. Comparison of the geometries of **1a** and **1d** [5] shows that the influence of the amino group on the geometry of the remaining part of the molecule is negligible. So, e.g., the changes in bond lengths upon substitution of the NH_2 group by hydrogen do not exceed 0.5 pm (cf. Table 9).

In the case of bridged structure **2a**, the ^{3}C^{4}C^{5}N segment of the molecule is distinctly bent and deviates about 19° from linearity. As a result, the CN multiple bond in **2a** is somewhat shortened, while the length of the CC bond is slightly increased compared with lithiated ketenimines **1a** and **1c**. The Li atom of **2a** lies approximately in the plane defined by the atoms ^{5}N, ^{4}C, and ^{3}C, its perpendicular distance from this plane being only about 6 pm (cf. Figure 2). Next neighbour of the lithium atom is ^{4}C. With 197.6 pm at the 6-31 G* level, the ^{7}Li–^{4}C bond is even shorter than the Li–C single bond in methyllithium (6-31 G*: 200.1 pm [28]).

To estimate the influence of the amino group in **2a** on the geometry of the remaining part of the molecule the structure of this part might be compared with the 6-31 G* data for **2b** [5]. Replacement of the NH_2 group by a hydrogen atom leaves the nitrogen carbon skeleton of the molecule virtually unchanged while the position of the lithium atom is shifted in that one carbon lithium bond length is somewhat reduced while the other is slightly increased (cf. Table 10).

The geometry optimization of **3a** has been performed under constraint of D_{2h} symmetry and the resulting stationary point turned out to be a local minimum (cf. Tables 8 and 11). According to the X-ray data a well as to our theoretical results the four-membered ring is essentially planar. Repulsive interactions between the bulky substituents in **A** or packing forces in the solid state might at least in part account for the remarkable differences between experimentally determined structural parameters and those calculated for **3a**. So, e.g., the experimental Li–N bond length exceeds our theoretical value by more than 10 pm. While calculated and experimental N–N distances are not too different, the experimental Li–Li separation is significantly wider (30 pm) than its computational counterpart.

The ^{3}C^{2}N^{1}Li moiety which is linear in **1d** is distinctly bent in dimer **3a**.

To evaluate the influence of electron correlation on the geometry of the nonclassical structure **2b** we reoptimized this molecule including correlation energy calculated by means of Møller-Plesset perturbation theory to the second order. The resulting structure ($E_{tot} = -139.22292$ a.u.) is shown along with the corresponding HF/6-31 G* result in Fig. 6 of the appendix. Comparison of the two geometries reveals that the principal features of the nonclassical molecule are retained upon optimization including correlation corrections.

While in the case of the lithiated ketenimine the *ab initio* (**1a**) and the semiempirical (**1a′**) structure are quite similar, marked differences occur between **2a** and **2a′** (cf. Tables 12 and 13).

3.3. Charge Distributions and Molecular Orbitals

The Mulliken charges of **1a** and **2a** calculated with the different basis sets at the corresponding optimized geometries are listed in Table 4a–b. The resulting dipole moments of **1a**–**1d** and **2a** are given in Table 5. Both, in **1a** as well as in **2a**, the general charge distribution is $(H_2N)(H)C^{\delta-}C^{\delta+}N^{\delta-}Li^{\delta+}$. Consequently, the nucleophilic centers of the CCNLi backbone are the nitrogen atom and the carbon atom carrying the amino group.

With all basis sets the HOMO of **1a** is a π orbital with the largest coefficients at ^{4}C and smaller ones at

Table 4a. Charge distributions in **1a** (in e_0) calculated at the corresponding optimized geometries.

Atom	STO-3G	6-31G	6-311G	6-31G*
^{1}Li	+0.3153	+0.7218	+0.7377	+0.6399
^{2}N	−0.3214	−0.8108	−0.6940	−0.8287
^{3}C	+0.1716	+0.3283	+0.1881	+0.5212
^{4}C	−0.1097	−0.1421	−0.1534	−0.2960
^{5}N	−0.3764	−0.8702	−0.8348	−0.8320
^{6,7}H	+0.1400	+0.3132	+0.2975	+0.3235
^{8}H	+0.0406	+0.1466	+0.1614	+0.1485

Table 4b. Charge distributions in **2a** (in e_0) calculated at the corresponding optimized geometries.

Atom	STO-3G	6-31G	6-311G	6-31G*
^{1,6}H	+0.1479	+0.3234	+0.3078	+0.3375
^{2}N	−0.3738	−0.8465	−0.8153	−0.8268
^{3}C	−0.0417	−0.2739	−0.3392	−0.2952
^{4}C	+0.0576	+0.1854	+0.1148	+0.3906
^{5}N	−0.2341	−0.4631	−0.4189	−0.5573
^{7}Li	+0.2347	+0.5948	+0.6707	+0.4491
^{8}H	+0.0614	+0.1564	+0.1725	+0.1646

Table 5. Dipole moments of **1a**–**1d**, **2a**, **1a′**, and **2a′** (in D) calculated at the corresponding optimized geometries.

Molecule	STO-3G	6-31G	6-311G	6-31G*	MNDO
1a	4.12	6.94	6.88	6.96	–
1b	4.24	–	–	–	–
1c	6.37	8.41	8.59	9.29	–
1d	–	–	–	8.02	–
2a	3.40	5.52	5.20	4.90	–
1a′	–	–	–	–	8.05
2a′	–	–	–	–	5.40

^{2}N, while the charge of this nitrogen atom is much more negative than that of ^{4}C. In addition calculations at the STO-3G level with full geometry optimization yield a positive Mulliken charge ($0.2792\,e_0$) at the carbon atom of the carbonyl group in acetyl chloride ($E_{tot} = -604.96688$ a.u.), while the carbon atom in methyl iodide ($E_{tot} = -6889.83985$ a.u.) is charged negatively ($-0.2725\,e_0$). Thus, the observed regioselectivity in the reactions of the lithiated aminonitriles with H_3CCOCl and H_3CI can be explained in terms of charge control (hard-hard interaction) in the first and orbital control (soft-soft interaction) in the second case. The same holds for **2a**, where the coefficients in the HOMO are larger at ^{3}C than at ^{5}N, while the negative charge of the nitrogen is stronger than that of the carbon atom.

Table 6. HF/6-31G*//6-31G* charge distributions in **1d** and **3a** (in e_0).

3a		**1d**	
Atom	q	Atom	q
$^{1,1'}$Li	+0.6375	^{1}Li	+0.6449
$^{2,2'}$N	−0.8924	^{2}N	−0.8250
$^{3,3'}$C	+0.5137	^{3}C	+0.4964
$^{4,4'}$C	−0.6293	^{4}C	−0.6512
$^{5,5',6,6'}$H	+0.1853	^{5,6}H	+0.1674

Analysis of the molecular orbitals of **1a** and **2a** as calculated with the 6-31G* basis set at the corresponding optimized geometry reveals that the valence orbitals of lithium are only weakly involved in occupied MOs. The HOMO of **1a**, which is of π symmetry, is bonding between ^{4}C and ^{3}C as well as between ^{2}N and ^{1}Li, but antibonding between ^{3}C and ^{2}N. Bonding participation of the lithium atom in this molecular orbital reflects the aforementioned donation of electron density from nitrogen into a vacant 2p orbital of the metal atom.

Mulliken charges of **3a** and **1d** are given in Table 6. The atomic charges in **1d** are very similar to those of the corresponding atoms in its dimer **3a**. Again the Mulliken charges of the nitrogen atoms ^{2}N and $^{2'}$N in the dimer are more negative than those of ^{4}C and $^{4'}$C, while the carbon atoms have larger orbital coefficients in the HOMO.

3.4. Dimerization

We further studied the dimerization reaction of lithiated aminonitriles. Assuming that replacement of the NH_2 group by hydrogen does not affect the dimerization reaction too severely, we used **3a**, the dimer of parent **1d**, in this part of the study. The 6-31G* optimized structures of **1d** and **2b** as well as their total energies at the HF/6-31G*//6-31G* and MP2/6-31G*//6-31G* level have been published recently and the data for these molecules have been taken from literature [5]. Using the HF/6-31G*//6-31G* total energies we calculate a dimerization energy of −58.7 kcal/mol relative to **1d**, which is rather close to the MNDO result of −52.9 kcal/mol [5]. Inclusion of electron correlation (MP2/6-31G*//6-31G*) slightly decreases the energy of reaction to −60.5 kcal/mol. Addition of HF/6-31G*//6-31G* zero point energy finally yields a value of −58.0 kcal/mol. Choosing the more stable monomer **2b** as reference yields a dimer-

ization energy of −41.1 kcal/mol without and of −40.0 kcal/mol including HF/6-31G*//6-31G* zero point energy. These reaction energies indicate that at least in the gasphase dimerization is an energetically favoured process.

To estimate the influence of the solvent we calculated the change of energy associated with the reaction [5]:

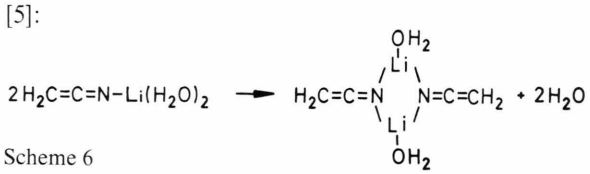

Scheme 6

At the HF/6-31G*//6-31G* level we obtained a value of −15.1 kcal/mol indicating that the dimerization remains exothermic in solution.

3.5. *Vibrational Spectra*

The vibrational frequencies of **1a**, **1c**, and **2a** calculated with the 6-31G and 6-31G* basis sets which are listed in Table 7 are schematically plotted in Fig. 4a, while those of **1d** and **3a** are compiled and drawn in Table 8 and Fig. 4b, respectively.

The monomers under consideration are either of C_s (**1a**, **1c**, **2b**) C_1 (**2a**), or of C_{2v} symmetry (**1d**). Thus in principle all fundamentals of **1a**, **1c**, **2a**, and **2b** should be active in IR. For **1a** and **1c** one expects twelve genuine vibrations of A′ and six of A″ symmetry. The A′ vibrations at 2304.1 cm^{-1} in **1a** and 2285.7 cm^{-1} in **1c** are predominantly due to stretching of the $^2N^3C$ bonds. The corresponding vibration in **2a** occurs at 2348.9 cm^{-1}. The shift of this vibration to shorter wavelengths compared with **1a** and **1c** indicates the expected higher triple bond character in **2a** which is also reflected by the shorter CN multiple bond length (cf. Tables 9–10). Due to their localization in the CN region these vibrations show a significant isotopic shift upon replacement of the corresponding nitrogen or carbon atom by its heavier isotop. In the case of **1d** we expect twelve genuine vibrations: five of A_1, three of B_1, and four of B_2 symmetry. The calculated stretching frequency of the CN bond is 2298.9 cm^{-1}.

The dimer **3a** is of D_{2h} symmetry. Thus, the vibrations which are active in IR should be inactive in a Raman spectrum and *vice versa*. In the case of **3a** one expects thirty genuine normal vibrations, six of A_g, four of B_{1g}, four of B_{2g}, one of B_{3g}, one of A_u, five of B_{1u}, four of B_{2u}, and five of B_{3u} symmetry. The first four classes comprise those vibrations only active in Raman, while the members of the last three are active in IR, only. The A_u mode is neither active in IR nor in Raman. The centrosymmetry might be more or less disturbed in dimers with substituents like **A**, **B**, and **C** and those vibrations which are of zero IR intensity in the idealized D_{2h} case should in principle become observable in the infrared spectrum, too.

In the case of **3a** antisymmetric stretching of the CN bonds (B_{3u}) occurs at 2245.2 cm^{-1} indicating that dimerization shifts the characteristic absorption of lithiated acetonitrile about 54 cm^{-1} to longer wavelengths.

Table 7. Vibrational frequencies of **1a**, **1c** and **2a** (in cm^{-1}) calculated at the corresponding optimized geometries.

No.	**1a** (C_s)	**1c** (C_s)	**2a** (C_1)
	6-31G ^{14}N	6-31G ^{14}N	6-31G ^{14}N
1	119.7 A′	124.1 A′	122.5
2	142.8 A″	137.5 A″	169.0
3	307.5 A′	235.0 A′	265.2
4	349.5 A″	310.8 A″	313.1
5	581.4 A′	314.5 A′	529.1
6	662.8 A″	657.9 A″	620.6
7	664.6 A″	665.9 A″	695.3
8	670.0 A′	672.7 A′	737.9
9	808.1 A′	799.9 A′	815.1
10	1125.2 A′	1148.8 A′	1063.9
11	1279.4 A″	1248.4 A″	1243.1
12	1350.7 A′	1362.7 A′	1292.6
13	1557.8 A′	1534.4 A′	1491.5
14	1845.3 A′	1823.6 A′	1854.2
15	2276.4 A′	2264.0 A′	2299.3
16	3304.2 A′	3342.1 A′	3244.7
17	3769.9 A′	3811.7 A′	3767.0
18	3879.2 A″	3935.1 A″	3907.9

No.	**1a** (C_s)		**1c** (C_s)		**2a** (C_1)	
	6-31G*		6-31G*		6-31G*	
	^{14}N	^{15}N	^{14}N	^{15}N	^{14}N	^{15}N
1	85.1 A′	84.6 A′	94.6 A″	94.6 A″	150.3	150.2
2	95.1 A″	93.9 A″	97.4 A′	97.4 A′	229.4	227.7
3	286.1 A′	282.6 A′	247.1 A″	247.1 A″	278.1	275.0
4	293.5 A″	293.1 A″	270.9 A′	270.9 A′	342.8	342.1
5	580.1 A″	580.0 A″	564.9 A″	564.9 A″	518.2	516.0
6	650.3 A′	649.9 A′	649.6 A″	649.6 A″	647.6	645.3
7	658.2 A″	654.7 A″	658.8 A′	658.8 A′	765.8	764.6
8	763.9 A′	761.9 A′	772.4 A′	772.4 A′	808.3	806.1
9	948.8 A′	947.2 A′	887.0 A′	887.0 A′	942.7	941.0
10	1118.0 A′	1114.0 A′	1154.2 A′	1154.2 A′	1081.7	1079.4
11	1315.8 A′	1309.8 A′	1313.6 A″	1313.6 A″	1237.9	1235.0
12	1319.9 A″	1319.9 A″	1334.4 A′	1334.4 A′	1328.4	1328.4
13	1568.7 A′	1563.3 A′	1522.3 A′	1522.3 A′	1500.0	1499.6
14	1840.8 A′	1840.5 A′	1833.3 A′	1833.3 A′	1847.6	1847.5
15	2304.1 A′	2280.4 A′	2285.7 A′	2285.7 A′	2348.9	2318.4
16	3324.8 A′	3324.8 A′	3373.8 A′	3373.8 A′	3249.4	3249.4
17	3707.1 A′	3707.1 A′	3719.5 A′	3719.5 A′	3711.2	3711.2
18	3776.1 A″	3776.1 A″	3794.1 A″	3794.1 A″	3806.7	3806.7

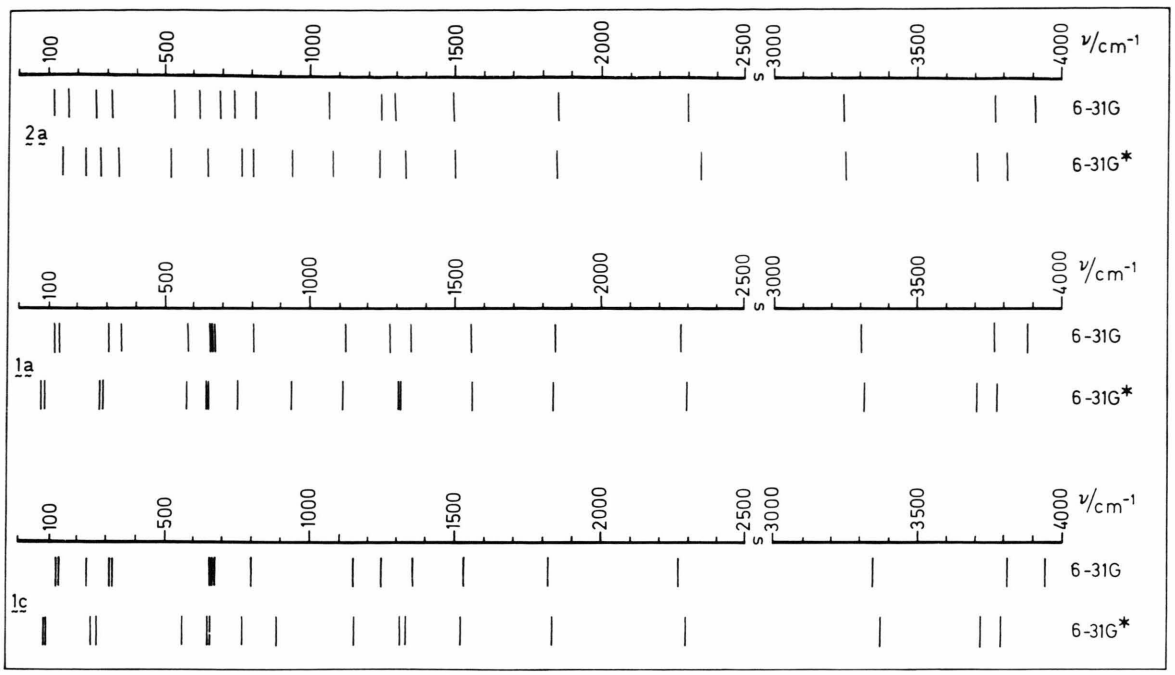

Fig. 4a. Vibrational frequencies (^{14}N) of **1a**, **1c**, and **2a** calculated at the HF/6-31G//6-31G and HF/6-31G*//6-31G* level.

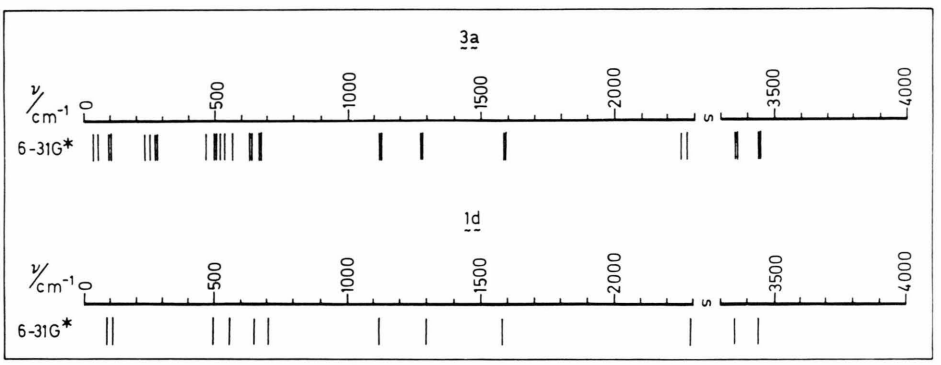

Fig. 4b. Vibrational frequencies (^{14}N) of **1d** and **3a** calculated at the HF/6-31G*//6-31G* level.

Scaling of the calculated CN stretching frequencies of **1a**, **1c**, **1d**, **2a**, **2b**, and **3a** with an empirical factor of 0.89 [30, 31] yields values of 2051, 2034, 2046, 2091, 2104, and 1998 cm^{-1}, respectively. Except those of **2a** and **2b** these scaled wavenumbers are rather close to the experimental data obtained for our lithiated aminonitriles (*vide infra*) and also for the dimer of lithiated phenyl acetonitrile [6]. Taking into account the expected relative stability of the ketenimine-like and the nonclassical structure in solution we discard **2a** and **2b** from our further considerations.

The 1800–2500 cm^{-1} regions of the experimental IR spectra of **A**, **B**, **C** and **D**, are shown in Figure 5. Like the spectra of other metalated nitriles [11, 12, 32–35] they are characterized by strong bands in the 2000–2100 cm^{-1} region, which in accordance with our theoretical results are usually assigned to stretching of the CN multiple bond. The spectra of all four compounds show absorptions somewhat above 2100 cm^{-1} (c). In the case of lithiated acetonitrile (**D**) this band occurs at 2134 cm^{-1} and had also been observed by Juchnovski et al. [11]. Based on their

Table 8. HF/6-31 G*//6-31 G* vibrational frequencies of **1d**, **2b**, and **3a** (in cm^{-1}).

No.	**1d**		**2b**		**3a**	
	^{14}N	^{15}N	^{14}N	^{15}N	^{14}N	^{15}N
1	91.7	90.4 B_1	212.8	210.9 A′	36.3	36.1 B_{1u}
2	111.6	110.0 B_2	432.6	430.7 A″	56.0	55.4 B_{2u}
3	494.9	491.6 B_2	512.3	510.5 A′	95.2	92.9 B_{2g}
4	554.3	554.3 B_1	529.6	528.1 A″	100.6	98.6 B_{1g}
5	649.1	645.0 B_1	763.6	761.7 A′	229.9	227.5 A_g
6	706.5	706.2 A_1	818.3	818.2 A′	249.7	249.7 A_u
7	1122.4	1121.9 B_2	1094.5	1085.1 A′	272.9	272.9 B_{3g}
8	1294.6	1279.3 A_1	1194.1	1193.8 A″	280.4	278.4 B_{1u}
9	1581.7	1580.0 A_1	1593.3	1593.2 A′	464.9	462.6 B_{2u}
10	2298.9	2274.7 A_1	2363.5	2332.2 A′	496.2	492.8 B_{2g}
11	3352.5	3352.5 A_1	3287.4	3287.4 A′	502.8	498.6 B_{1u}
12	3439.0	3439.0 B_2	3358.8	3358.8 A″	519.7	518.4 B_{1g}
13					536.8	536.6 A_g
14					566.9	566.3 B_{3u}
15					635.1	635.1 B_{1g}
16					635.7	635.6 B_{2u}
17					670.3	664.5 B_{1g}
18					677.1	670.9 B_{2u}
19					1120.8	1120.4 B_{2g}
20					1120.9	1120.4 B_{1u}
21					1278.8	1263.2 B_{3u}
22					1278.9	1263.3 A_g
23					1581.7	1579.9 B_{3u}
24					1582.1	1580.3 A_g
25					2245.2	2223.9 B_{3u}
26					2273.8	2251.6 A_g
27					3355.3	3355.3 B_{3u}
28					3355.4	3355.4 A_g
29					3444.4	3444.4 B_{2g}
30					3444.4	3444.4 B_{1u}

experimental results those authors assign this absorption to the lithium derivative of the acetonitrile dimer [11]. The corresponding weak bands in the spectra of compounds **A**, **B**, and **C** gain intensity when the sample is briefly exposed to air while the strong absorptions between 2000 and 2100 cm^{-1} decrease simultaneously. Thus, we assign the weak bands to oxidation or hydrolysis products of the lithiated aminonitriles or to compounds formed from these products in subsequent reactions.

In the cases of **A** and **B** the strong absorptions occur at 2061 and 2016 cm^{-1}, and the 2061 cm^{-1} band of **A** has a shoulder at about 2025 cm^{-1} (spectrum a). For compound **C** the characteristic absorption is significantly split with absorption maxima of almost equal intensity at 2019 and 2034 cm^{-1}. Of special interest is the question as to the origins of the shoulder and the splitting. A similar splitting as for compound **C** has previously been observed for lithiated acetonitrile **D** in THF. These two absorptions have been assigned to the free ion and a solvent-separated ion pair [11, 12]. In the solid state, however, a single broad band had been obtained for the same compound [11]. Subsequent studies revealed, however, that lithiated acetonitrile in THF is a dimer between room temperature and the melting point of the solvent [5]. Since other authors [33] report a single band at 2040 cm^{-1} for lithiated acetonitrile we metalated acetonitrile employing lithium diisopropylamide, and the corresponding spectrum is shown together with those of **A**, **B**, and **C** in Figure 5. Different from the results given in [11] we obtain a sharp band at 2051 cm^{-1} and in addition an absorption of much lower intensity at about 2080 cm^{-1}. Qualitatively the same result is obtained when the lithiation is carried out with either *n*- or *tert*-butyllithium. Since lithiated acetonitrile is known to be a dimer in solution we assign the intense absorption at 2051 cm^{-1} to **3a**. According to our calculations the band due to monomer **1d** is expected to occur at higher wavenumbers (cf. Table 8) than the one belonging to **3a**. Thus, we assign the weak absorption at 2080 cm^{-1} to small amounts of the monomer **1d**.

When the reaction mixture containing **A** is kept under argon at room temperature for four hours, the shoulder at 2025 cm^{-1} in its IR spectrum is replaced by a strong band of almost the same intensity as the absorption at 2061 cm^{-1} (spectrum b). Since it is known that the major amount of **A** is monomeric under the conditions of the cryoscopic measurement, we assign the absorption at 2061 cm^{-1} to the monomer and the one at 2025 cm^{-1}, which grows in upon standing at room temperature to the dimer. This assignment concurs with the computational results as far as the relative positions of the CN stretching vibrations of monomers and dimers are concerned. Thus, it seems as if significant dimerization of **A** does not take place under the conditions of the cryoscopic measurement but occurs at room temperature. Assuming that the coordination number of the lithium atom is the same in the monomer and the dimer (cf. Scheme 6) the number of molecules is higher on the side of the dimer. Thus it might be argued that as far as entropy is concerned dimerization is indeed preferred at higher temperatures [4, 5]. Analogue cases are described in literature [4].

As yet no cryoscopic data are available for compounds **B** and **C**. The characteristic absorption of **B** has a sharp maximum at 2016 cm^{-1} and a very weak shoulder at about 2060 cm^{-1} (s). We assign the sharp band at 2016 cm^{-1} to the dimer, while the shoulder

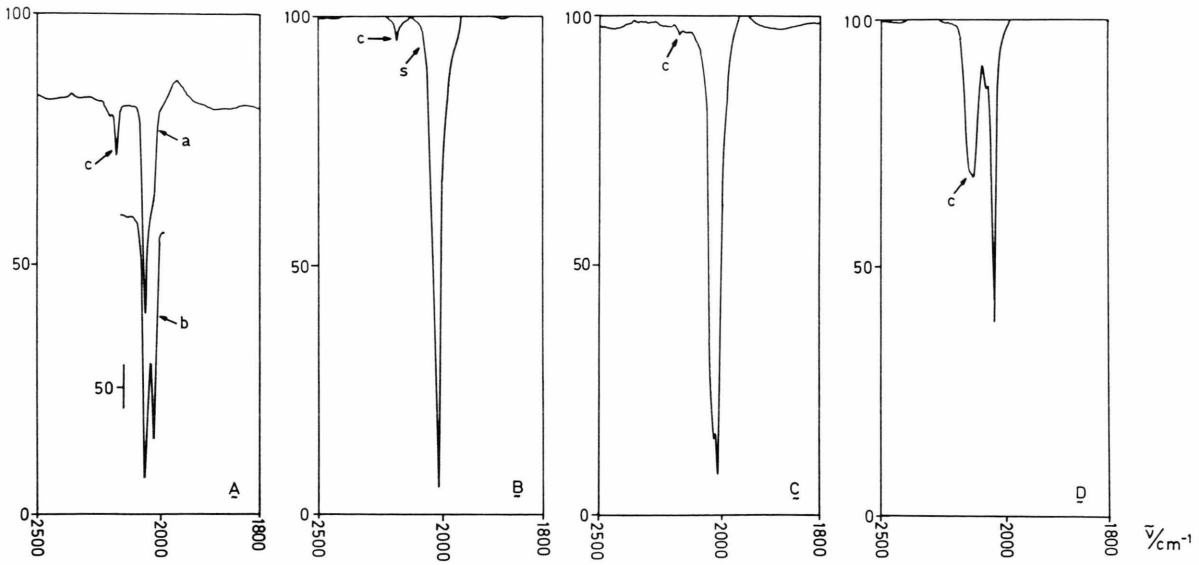

Fig. 5. IR spectra of **A**, **B**, **C**, and **D**. The absorptions labeled c are due to sideproducts. Spectrum a has been recorded immediately after mixing of the reactands, spectrum b after the reaction mixture had been kept four hours at room temperature. s in the spectrum of **B** indicates a weak shoulder.

indicates the presence of small amounts of the monomer.

As already mentioned the corresponding absorption of **C** is distinctly split with peaks at 2019 and 2034 cm^{-1}. Due to their position we assign these bands to the dimer.

At the moment we are unable to provide a definite explanation for the splitting of the band in **C**. This splitting is much smaller than in the case of, e.g., compounds **A** and **D**. To check whether the two bands indicate simultaneous presence of the *cis*- and the *trans* form of the dimer, we calculated the vibrational frequencies for these two isomers with the MNDO method. According to these calculations the characteristic vibrations of both isomers should be observed at virtually the same wavenumber. Thus, it is doubtful whether the observed splitting of 15 cm^{-1} is due to presence of both isomers. Both absorptions disappear simultaneously upon hydrolysis indicating that they might belong to one and the same species.

4. Experimental Part

Preparation of the lithiated nitriles requires highly anhydrous conditions. All flasks were dried by heating in vacuum and subsequently filled with dry argon (blue gel). The reactions were carried out under a slight pressure of dry argon and all ingredients were added by syringe through septa. THF stored over KOH was freshly distilled from NaH in an argon atmosphere prior to use.

5.5 mmol n-butyllithium in n-hexane were added dropwise to a solution of 0.56 g (5.5 mmol) diisopropylamine in 10 ml dry THF at −78 °C. The solution was warmed to 0 °C and then cooled again to −78 °C. 5 mmol of the nitrile (pure or dissolved in 5 ml dry THF) were added slowly. After stirring for thirty minutes the mixture was warmed up to room temperature.

IR spectra were recorded on a Perkin-Elmer FT 1750 Fourier transform spectrometer. The cells have been purged with argon before being filled.

5. Appendix

Table 9. Structural parameters of **1a**, **1b**, and **1c** calculated at the HF level. Bond lengths in pm, bond angles in degrees.

1a	STO-3G	STO-6G	6-31G	6-311G	6-31G* [e]
$r(^1Li-^2N)$	163.3	163.0	174.6	172.4	176.1 (176.2)
$r(^2N-^3C)$	121.0	121.0	119.3	118.9	118.1 (118.2)
$r(^3C-^4C)$	131.8	131.7	133.7	133.6	133.5 (133.2)
$r(^4C-^8H)$	108.1	107.7	107.5	107.3	107.7 (107.2)
$r(^4C-^5N)$	146.4	146.1	142.6	143.1	143.3
$r(^5N-^7H)$	103.5	103.1	99.5	99.4	100.2
$r(^5N-^6H)$	103.5	103.1	99.5	99.4	100.2
$\angle(^1Li^2N^3C)$	176.4	176.4	177.3	176.8	172.7
$\angle(^4C^3C^2N)$	179.4	179.3	179.3	179.7	179.2
$\angle(^8H^4C^5N)$	120.4	120.2	121.3	121.2	122.1
$\angle(^8H^4C^3C)$	119.2	119.3	118.3	118.7	118.4 (120.1)
$\angle(^5N^4C^3C)$	120.3	120.4	120.4	120.1	119.5
$\angle(^7H^5N^6H)$	104.1	104.2	113.6	112.9	107.5
1b	STO-3G	STO-6G			
$r(^1Li-^2N)$	163.0	162.9			
$r(^2N-^3C)$	121.3	121.3			
$r(^3C-^4C)$	131.3	131.4			
$r(^4C-^8H)$	107.8	107.5			
$r(^4C-^5N)$	147.4	147.2			
$r(^5N-^7H)$	103.3	102.9			
$r(^5N-^6H)$	103.6	103.2			
$\angle(^1Li^2N^3C)$	176.9	176.7			
$\angle(^4C^3C^2N)$	177.0	177.1			
$\angle(^8H^4C^5N)$	118.1	118.1			
$\angle(^8H^4C^3C)$	120.1	120.2			
$\angle(^5N^4C^3C)$	121.6	121.6			
$\angle(^7H^5N^6H)$	104.0	104.1			
1c	STO-3G	STO-6G	6-31G	6-311G	6-31G*
$r(^1Li-^2N)$	163.3	163.0	174.7	172.4	176.2
$r(^2N-^3C)$	121.2	121.1	119.4	119.1	118.3
$r(^3C-^4C)$	131.7	131.6	133.7	133.6	133.4
$r(^4C-^8H)$	107.9	107.6	107.2	107.0	107.3
$r(^4C-^5N)$	146.6	146.3	142.2	142.9	143.6
$r(^5N-^7H)$	103.5	103.0	99.2	99.2	100.1
$r(^5N-^6H)$	103.5	103.0	99.2	99.2	100.1
$\angle(^1Li^2N^3C)$	179.6	179.7	179.0	179.6	178.4
$\angle(^4C^3C^2N)$	179.4	179.5	179.6	180.0	179.6
$\angle(^8H^4C^5N)$	116.7	116.6	119.1	118.5	117.9
$\angle(^8H^4C^3C)$	119.4	119.4	118.6	118.5	118.7
$\angle(^5N^4C^3C)$	124.0	123.9	122.3	123.0	123.4
$\angle(^7H^5N^6H)$	104.4	104.6	115.9	114.6	108.1

[e] The values in parentheses are 6-31G* data for **1d** (C_{2v}) taken from [5].

Table 10. Structural parameters of **2a** calculated at the HF level. Bond lengths in pm, bond angles in degrees.

2a	STO-3G [f]	STO-6G	6-31G	6-311G	6-31G* [g]
$r(^1H-^2N)$	103.3	102.9	99.7	99.6	100.3
$r(^2N-^3C)$	149.3	148.7	144.4	144.7	144.8
$r(^3C-^4C)$	145.3 (143.4)	144.9	141.4	140.2	140.8 (140.7)
$r(^4C-^5N)$	118.2 (118.0)	118.2	117.0	116.9	116.0 (115.9)
$r(^3C-^8H)$	108.9 (108.1)	108.4	108.1	107.9	108.3 (107.9)
$r(^2N-^6H)$	103.3	102.9	99.3	99.2	99.9
$r(^5N-^7Li)$	201.7	199.9	229.1	214.2	212.7
$r(^3C-^7Li)$	207.8 (205.6)	206.7	216.3	218.9	220.7 (215.9)
$r(^4C-^7Li)$	189.9 (188.9)	188.6	204.8	197.9	197.6 (199.4)
$\angle(^2N^3C^4C)$	113.8	114.5	115.7	116.2	115.0
$\angle(^8H^3C^7Li)$	120.4	120.0	120.5	120.5	121.5
$\angle(^2N^3C^7Li)$	129.0	128.8	113.5	114.2	115.2
$\angle(^4C^3C^7Li)$	62.1	62.0	66.0	62.4	61.7
$\angle(^3C^7Li^5N)$	77.5	78.0	69.8	71.5	71.4
$\angle(^1H^2N^6H)$	103.6	104.0	112.9	112.0	107.2
$\angle(^3C^4C^5N)$	153.3 (155.6)	152.8	161.1	160.0	160.4 (160.1)
$\angle(^2N^3C^8H)$	108.7	108.9	117.2	117.5	117.7
$\angle(^8H^3C^4C)$	110.5	110.7	113.8	114.3	113.1 (114.6)

[f] The values in parentheses are STO-3G data for **2b** taken from [36].

[g] The values in parentheses are 6-31G* data for **2b** taken from [5].

Table 11. HF/6-31G* geometries of **3a** and **1d** in comparison with experimental average values (X-ray) obtained from dimeric **A** (**3**) in the solid state. Bond lengths in pm, bond angles in degrees.

	3a	**3**	**1d**
$r(^2N-^{2'}N)$	300.1	303.3	–
$r(^1Li-^{1'}Li)$	246.4	276.0	–
$r(^1Li-^2N)$	194.2	205.0	176.2
$r(^2N-^3C)$	119.0	118.3	118.2
$r(^3C-^4C)$	132.5	137.8	133.2
$r(^4C-^{5,6}H)$	107.2	–	107.2
$\angle(^2N^1Li^{2'}N)$	101.2	95.5	–
$\angle(^1Li^2N^{1'}Li)$	78.8	84.6	–
$\angle(^1Li^2N^3C)$	140.6	137.4	180.0
$\angle(^2N^3C^4C)$	180.0 [h]	178.0	180.0
$\angle(^5H^4C^6H)$	119.9	–	119.8
$\angle(^{5,6}H^4C^3C)$	120.1	–	120.1

[h] Not optimized (see text).

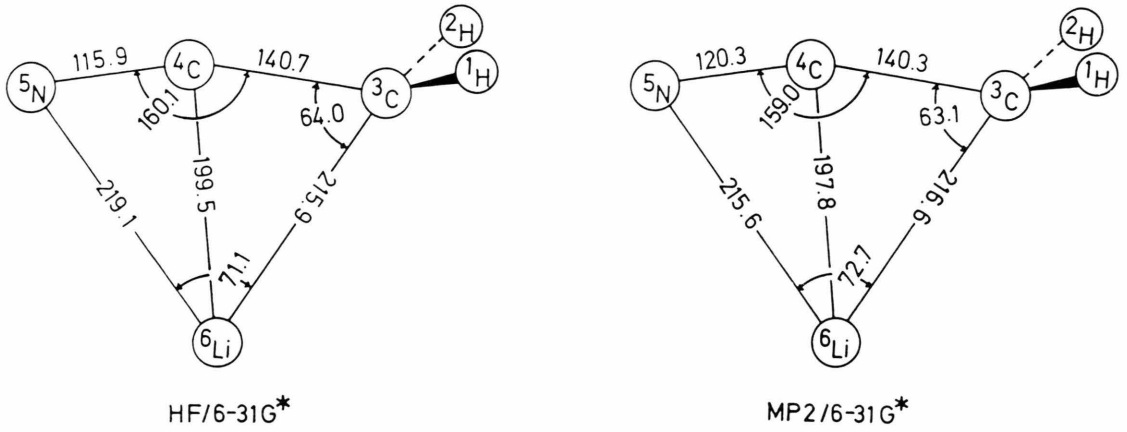

Fig. 6. HF/6-31G* and MP2/6-31G* optimized structures of **2b**.

$r(^1Li-^2N)$	178.6
$r(^2N-^3C)$	119.8
$r(^3C-^4C)$	134.5
$r(^4C-^8H)$	109.0
$r(^4C-^5N)$	142.9
$r(^5N-^7H)$	101.3
$r(^5N-^6H)$	101.3
$\angle(^1Li^2N^3C)$	176.0
$\angle(^4C^3C^2N)$	178.3
$\angle(^8H^4C^5N)$	120.6
$\angle(^8H^4C^3C)$	120.6
$\angle(^5N^4C^3C)$	118.8
$\angle(^7H^5N^6H)$	103.8

Table 12.
MNDO structural parameters of **1a'**. Bond lengths in pm, bond angles in degrees.

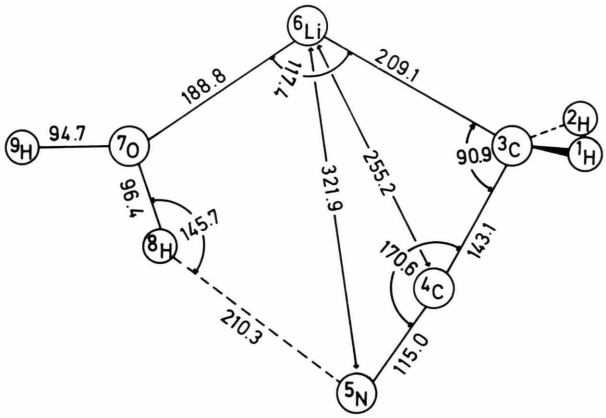

Fig. 7. HF/6-31G* optimized structure of **2b** · H_2O.

$r(^1H-^2N)$	101.4
$r(^2N-^3C)$	148.4
$r(^3C-^4C)$	145.5
$r(^4C-^5N)$	116.9
$r(^3C-^8H)$	110.9
$r(^2N-^6H)$	101.2
$r(^5N-^7Li)$	333.3
$r(^3C-^7Li)$	190.6
$r(^4C-^7Li)$	246.2
$\angle(^2N^3C^4C)$	112.7
$\angle(^3C^4C^5N)$	177.5

Table 13.
MNDO structural parameters of **2a'**. Bond lengths in pm, bond angles in degrees.

Acknowledgement

The authors gratefully acknowledge the computing time provided by the Rechenzentrum der Rheinisch-Westfälischen Technischen Hochschule Aachen and the access to a TRACE Supercomputer made possible by its vendor, the firm of GEI, Aachen and also the generous technical support by Dr. A. Oswald and Mr. M. Paulsen of GEI during our work on the TRACE.

[1] D. Enders, H. Kipphardt, and P. Gerdes, Angew. Chem. **102,** 226 (1990).
[2] G. Boche, D. Enders, P. Gerdes, M. Marsch, H. Ahlbrecht, and H. Sommer, in preparation.
[3] B. J. Wakefield, The Chemistry of Organolithium Compounds, Pergamon Press, Oxford 1973.
[4] W. Bauer and D. Seebach, Helv. Chim. Acta **67,** 1972 (1984).
[5] J. Kaneti, P. v. Ragué Schleyer, T. Clark, A. J. Kos, G. W. Spitznagel, J. G. Andrade, and J. B. Moffat, J. Amer. Chem. Soc. **108,** 1481 (1986).
[6] G. Boche, M. Marsch, and K. Harms, Angew. Chem. **98,** 373 (1986).
[7] G. Boche, Angew. Chem. **101,** 286 (1989).
[8] R. Das and C. A. Wilkie, J. Amer. Chem. Soc. **94,** 4555 (1972).

[9] P. Gerdes, Dissertation, RWTH Aachen 1989.
[10] D. Seebach, Angew. Chem. **100,** 1685 (1988).
[11] I. N. Juchnovski and I. G. Binev, J. Organomet. Chem. **99,** 1 (1975).
[12] I. N. Juchnovski, J. S. Dimitrova, I. G. Binev, and J. Kaneti, Tetrahedron **34,** 779 (1978).
[13] M. Dupuis, J. Rys, and H. F. King, QCPE **13,** 403 (1981).
[14] M. W. Schmidt, J. A. Boatz, K. K. Baldridge, S. Koseki, M. S. Gordon, S. T. Elbert, and B. Lam, QCPE **7,** 115 (1987).
[15] M. J. Frisch, J. S. Binkley, H. B. Schlegel, K. Raghavachari, C. F. Melius, R. L. Martin, J. J. P. Stewart, F. W. Bobrowicz, C. M. Rohlfing, L. R. Kahn, D. J. DeFrees, R. Seeger, R. A. Whiteside, D. J. Fox, E. M. Fleuder, and J. A. Pople, Gaussian 86, Carnegie-Mellon Quantum Chemistry Publishing Unit, Pittsburg PA, 1984.
[16] C. Møller and M. S. Plesset, Phys. Rev. **46,** 618 (1934).
[17] W. J. Hehre, R. F. Stewart, and J. A., Pople, J. Chem. Phys. **51,** 2657 (1969).
[18] J. S. Binkley, J. A. Pople, and W. J. Hehre, J. Amer. Chem. Soc. **102,** 939 (1980).
[19] W. J. Hehre, R. Ditchfield, and J. A. Pople, J. Chem. Phys. **56,** 2257 (1972).
[20] J. D. Dill and J. A. Pople, J. Chem. Phys. **62,** 2921 (1975).
[21] J. S. Binkley and J. A. Pople, J. Chem. Phys. **66,** 879 (1977).
[22] P. C. Hariharan and J. A. Pople, Theor. Chim. Acta **28,** 213 (1973).
[23] R. Krishnan, J. S. Binkley, R. Seeger, and J. A. Pople, J. Chem. Phys. **72,** 650 (1980).
[24] M. J. S. Dewar and W. Thiel, J. Amer. Chem. Soc. **99,** 4899 (1977).
[25] W. Thiel, QCPE **11,** 353 (1978).
[26] J. P. Stewart, QCPE **9,** 581 (1990).
[27] W. Thiel, QCPE **2,** 438 (1982).
[28] W. J. Hehre, L. Radom, R. v. Ragué Schleyer, and J. A. Pople, Ab initio Molecular Orbital Theory, John Wiley & Sons, New York 1986, p. 401 ff.
[29] E.-U. Würthwein, K. D. Sen, J. A. Pople, and P. v. Ragué Schleyer, Inorg. Chem. **22,** 496 (1983).
[30] S. Moran, H. B. Ellis Jr., D. J. DeFrees, A. D. McLean, and G. B. Ellison, J. Amer. Chem. Soc. **109,** 5996 (1987).
[31] D. J. DeFrees and A. D. McLean, J. Chem. Phys. **82,** 333 (1985).
[32] C. Krüger, J. Organomet. Chem. **9,** 125 (1967).
[33] G. A. Gornowicz and R. West, J. Amer. Chem. Soc. **93,** 1714 (1971).
[34] I. N. Juchnovski, I. G. Binev, and Ts. M. Kolev, Tetrahedron Lett. **18,** 1519 (1976).
[35] I. N. Juchnovski, V. B. Radomirska, I. G. Binev, and E. A. Grekova, J. Organomet. Chem. **128,** 139 (1977).
[36] J. B. Moffat, J. Chem. Soc., Chem. Commun. **1980,** 1108.